激光+GMAW 复合热源焊接过程热-力耦合数值分析

吴向阳[1]， 宿浩[2]， 孙岩[2]， 陈姬[2]， 武传松[2]
(1. 中车青岛四方机车车辆股份有限公司, 青岛, 266111; 2. 山东大学材料液固结构演变与加工教育部重点实验室焊接研究所, 济南, 250061)

摘要: 从宏观的焊接热过程出发, 根据激光+GMAW 复合热源焊接的特点, 提出了适用于复合热源焊接的“双椭球体 + 峰值递增圆柱体”组合式体积热源分布模式; 建立了激光+GMAW 复合热源焊接过程的有限元模型, 数值计算了焊接温度场和焊缝横截面的形状尺寸, 计算结果与试验结果吻合良好, 证明了组合式体积热源模型的合理性和适用性. 采用焊接温度场的计算结果, 进一步对复合热源焊接和 GMAW 的焊接变形和残余应力进行了数值模拟和对比分析. 结果表明, 在焊缝熔深基本相同的情况下, 复合热源焊接的焊接热输入、焊缝熔宽、焊接变形和高应力区域范围等均比 GMAW 小. 研究结果印证了激光+GMAW 复合热源焊接工艺的优越性, 并为焊接工艺参数的优化提供了基础理论数据.

创新点: (1) 建立了适用于激光+GMAW 复合焊接的组合式热源分布模式, 数值计算了焊件温度和残余应力分布.
(2) 激光+GMAW 的热输入、焊缝熔宽和高应力区范围均比相同熔深情况下的 GMAW 小, 印证了复合热源焊接的工艺优越性.

关键词: 复合焊接; 组合式体积热源; 热力耦合; 数值分析
中图分类号: TG 442 **文献标识码:** A **doi:** 10. 12073/j. hjxb. 20200708001

0 序 言

激光+GMAW(gas metal arc welding, 熔化极气体保护焊) 将激光和熔化极电弧这两种物理性质、能量传输机制截然不同的热源复合在一起[1-2], 充分利用两种热源各自的优点, 并有效地弥补了各自的不足, 目前已在工业领域获得了广泛的应用. 近年来, 研究者针对激光+GMAW 复合焊接工艺和焊接机理进行了大量的研究工作. 研究证实, 激光与 GMAW 复合作用可有效提高焊缝熔深, 且对间隙、错边和对中偏离的容忍度均较强[3], 电弧能够有效地提高被焊材料对激光能量的吸收能力[4]; 激光能够稳定电弧, 同时能够引导和收缩电弧, 且激光和电弧复合能够显著提高焊接速度[5].

近年来, 研究者针对激光焊和电弧焊进行了大量的建模计算研究, 分析了焊接温度场和应力应变场[6-8]. 虽然也开展了一些针对激光+GMAW 复合焊接过程的数值模拟研究[9], 但整体来看目前的研究还不够深入, 且复合焊接与 GMAW 在焊接变形和残余应力等方面的对比研究鲜有报道. 在激光+GMAW 复合焊接过程中, 由于激光与 GMAW 电弧相互作用的复杂性, 难以采用试验测试的方法对激光+GMAW 复合焊接过程中电弧和激光的特性进行精确测量. 因此, 从宏观传热过程出发, 不考虑复杂的激光小孔动力学特性, 以复合热源焊接的焊缝横断面形状尺寸为依据, 采用 SYSWELD 软件建立反映复合热源热力作用特点的体积热源模型, 并进行焊接温度场的计算; 在此基础上, 利用工件温度分布数据作为初始温度场进行应力应变的有限元数值计算, 为激光+GMAW 复合焊接工艺的优化提供基础理论数据.

1 复合热源温度场的数值计算

1.1 组合式体积热源模型

对于激光+GMAW 复合焊接来说, 由于焊缝下半部分体积较小且散热较块, 因此采用中心热流不变的作用模式很难计算得到理想的熔池轮廓. 考虑到激光与电弧之间的相互作用, 以及激光在小孔内

收稿日期: 2020 − 07 − 08

壁多次反射所起到的增强效果，采用峰值热流递增的热源，有效地对深度方向上的热流功率进行补偿．因此，根据激光+GMAW 复合热源焊接焊缝横断面几何形状的特点，建立“双椭球体热源+峰值递增圆柱体热源”的组合式体积热源模型．

热源上半部分采用双椭球体热源，即

$$q(x,y,z)=\frac{12\sqrt{3}Q\chi_1}{\pi\sqrt{\pi}a(b_1+b_2)c}\exp\left(\frac{-3x^2}{a^2}\right)\exp\left(\frac{-3y^2}{b_1^2}\right)\exp\left(\frac{-3z^2}{c^2}\right)(y<0,z\leqslant H_1) \tag{1}$$

$$q(x,y,z)=\frac{12\sqrt{3}Q\chi_1}{\pi\sqrt{\pi}a(b_1+b_2)c}\exp\left(\frac{-3x^2}{a^2}\right)\exp\left(\frac{-3y^2}{b_2^2}\right)\exp\left(\frac{-3z^2}{c^2}\right)(y\geqslant 0,z\leqslant H_1) \tag{2}$$

式中：Q 为总热源；a, b_1, b_2 和 c 均为半椭球体的分布参数．

热源下半部分采用热流递增的圆柱体热源，即

$$q_{V2}(r,z)=\frac{6Q\chi_2}{\pi r_0 H(mH+2r_0)}\exp\left(\frac{-3r^2}{r_0^2}\right)\left(\frac{mz+r_0}{r_0}\right)\quad(H_1<z\leqslant d) \tag{3}$$

式中：d 为板厚；H_1 为双椭球体热源的作用高度，m 为调节系数；H 为圆柱体热源的作用高度；r_0 为圆柱体热源的作用半径；χ_1 和 χ_2 分别为组合式热源上、下两部分的功率分配系数，有

$$\chi_1+\chi_2=1 \tag{4}$$

χ_1 和 χ_2 的取值依据电弧和激光的功率占比来确定，即

$$\chi_1=\frac{Q_A}{Q} \tag{5}$$

$$\chi_2=\frac{Q_L}{Q} \tag{6}$$

式中：Q_A 和 Q_L 分别是电弧和激光的功率．

1.2 材料热物性参数

试验中采用的被焊材料为 8 mm 厚 Q235 低碳钢板，其热物性参数中的综合散热系数、比热容、热导率和蒸发系数均随温度的变化而变化，如图 1 所示．模型中采用的其它参数取值如表 1 所示．

1.3 网格划分

为兼顾计算时间和计算精度，采用 6 节点的五面体网格．由于工件左右对称，因此模型在宽度方向上仅取一半进行计算．在不影响计算精度的前提下，长度方向上也按比例仅选取一部分进行计算．在温度梯度较大的熔池和热影响区采用较细密的

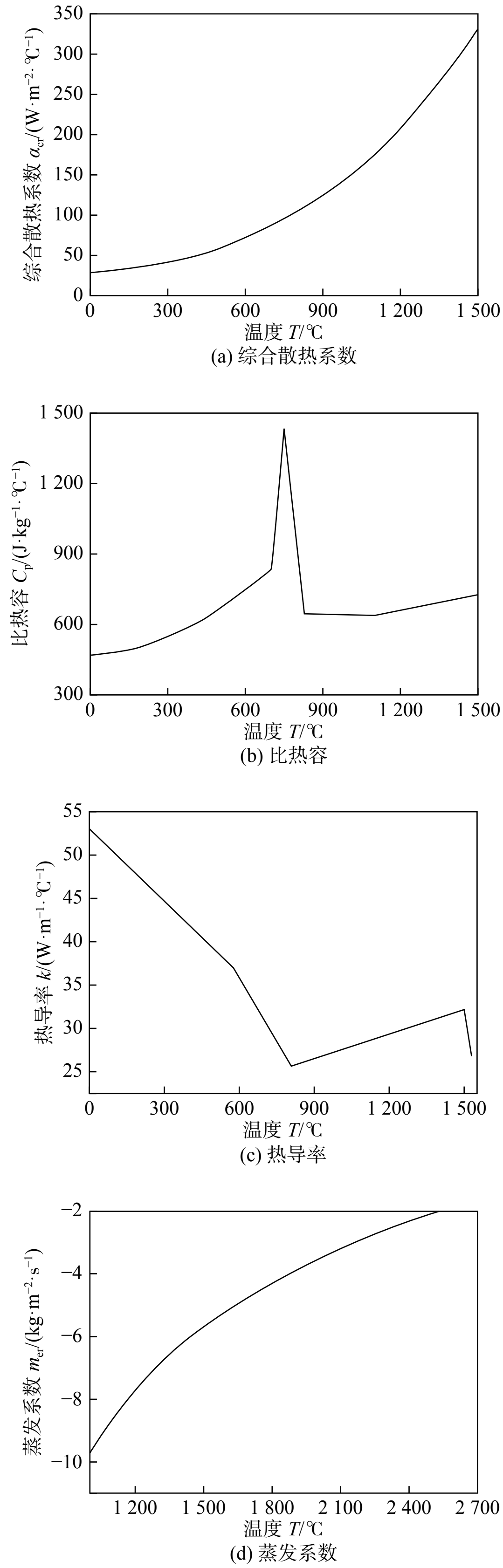

图 1 计算所采用的材料热物性参数

Fig. 1 Thermo-physical properties of the material used in the calculation. (a) heat transfer coefficient; (b) heat capacity; (c) heat conductivity; (d) evaporation coefficient

表 1　模型中的其它参数取值

Table 1　Other parameters used in the model

环境温度 T_∞/K	熔点 T_m/K	密度 ρ/(kg·m^{-3})	蒸发潜热 L_b/(10^5 J·kg^{-1})	重力加速度 g/(m·s^{-2})
293	1 773	6 900	73.43	9.8

网格，网格尺寸约为 0.1 mm；而在温度梯度小的区域采用较稀疏的网格，网格尺寸约为 0.8 mm. 这样即保证了工件上关键部位的计算精度，又减少了整体的节点数和计算迭代次数，提高了计算效率. 计算所采用的工件尺寸为 40 mm (长) × 10 mm (宽) × 8 mm (高)，网格划分如图 2 所示.

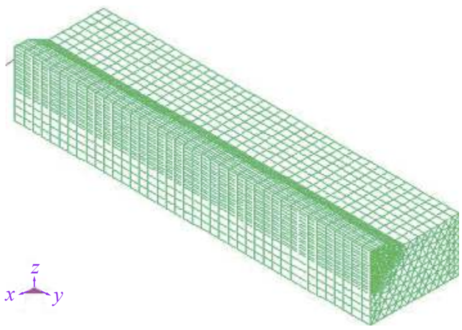

图 2　几何模型的网格划分

Fig. 2　Mesh generation of the geometric model

1.4　温度场计算结果与试验验证

模拟计算所采用的激光功率为 2 000 W，离焦量为 1 mm；焊丝直径为 1.2 mm，焊丝伸出长度为 16 mm；光丝夹角为 27.7°，光丝间距为 1 mm；熔滴过渡频率为 1 滴/脉冲，送丝速度为 6 200 mm/min，焊接电流为 173.3 A，电弧电压为 25.4 V，焊接速度为 1.0 m/min. 根据电弧和激光的功率比值确定 χ_1 和 χ_2 的取值分别为 0.68 和 0.32. 图 3 为计算所得到的温度分布图. 图 4 为采用组合式体积热源计算得到的焊缝横截面与试验结果的对比，可以看出计算所得的焊缝熔宽、熔深和熔合线走向等均与试验结果接近，模拟结果与试验结果吻合良好.

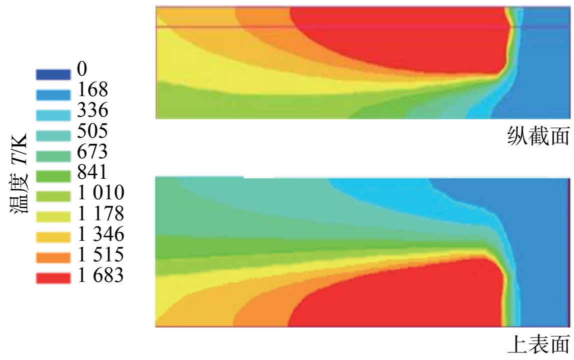

图 3　工件纵截面和上表面的温度分布图

Fig. 3　Temperature distribution of the longitudinal section and top surface of the workpiece

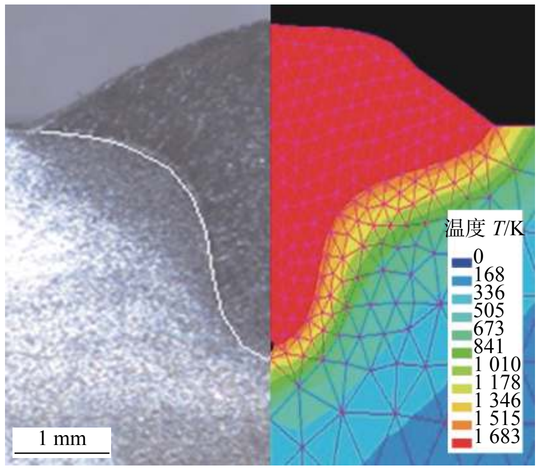

图 4　焊缝横截面的试验结果 (左) 和模拟结果 (右) 对比

Fig. 4　Comparison between the experimental and calculated results of the weld cross section

2　复合焊接热变形的数值分析

为比较激光+GMAW 复合热源焊接与常规 GMAW 焊接的热变形情况，针对 8 mm 厚低碳钢板在采用两种方法焊接时所产生的热变形进行比较，如表 2 所示. 可以看出，在获得基本相同焊缝熔深的情况下，GMAW 所需的焊接电流、电弧电压、送丝速度等均比激光+GMAW 高很多，而且焊缝熔宽尺寸也比复合热源焊接宽约 45.12%.

表 2　相同熔深情况下的 GMAW 和复合焊接参数

Table 2　Welding parameters of GMAW and laser + GMAW with similar weld penetration

工艺	电流I/A	电压U/V	送丝速度v_f/(m·min^{-1})	焊接速度v_0/(m·min^{-1})	熔宽w/mm	熔深h/mm
GMAW	427	35.3	14.2	1	11.00	2.90
激光+GMAW	173.3	25.4	6.2	1	7.58	2.91

2.1 力学性能参数

计算所采用材料的泊松比取值为 0.33，杨氏模量和屈服强度均随温度变化，取值如图 5所示. 工件的夹持情况如图 6 所示.

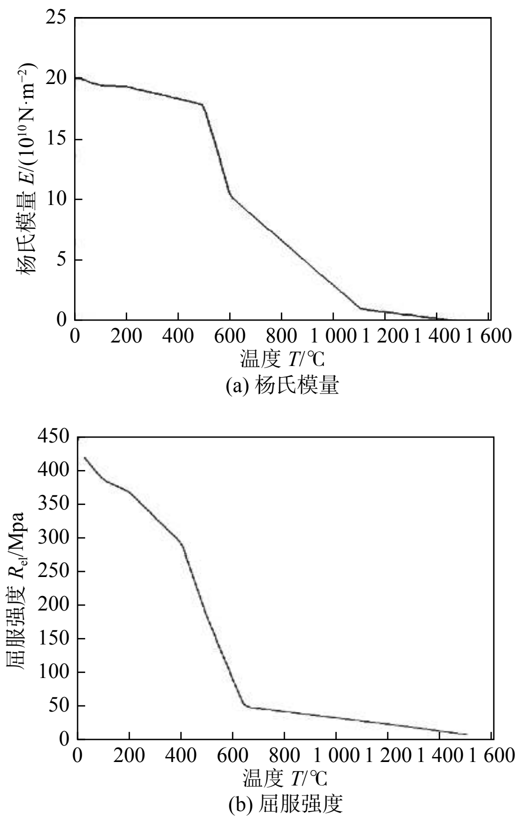

图 5 计算所采用的杨氏模量和屈服强度

Fig. 5 Young's modulus and yield strength used in the model. (a) Young's modulus; (b) yield strength

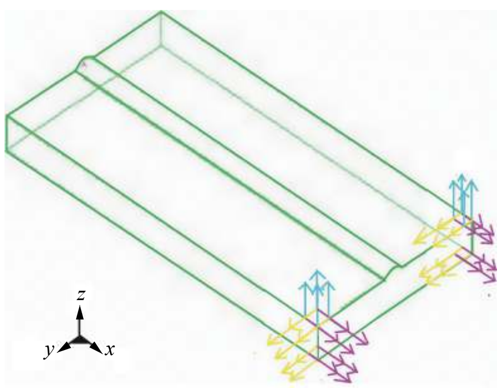

图 6 工件的夹持情况示意图

Fig. 6 Schematic diagram for the clamping situation of the workpiece

2.2 焊接变形

焊接完成后，立即松开夹具，让工件自由变形. 图 7 所示为焊后 300 s 工件的整体变形情况. 可以看出，在熔深基本相同的情况下，由于 GMAW 的焊接热输入比复合焊接高很多，因此 GMAW 所得到的工件最大变形量是复合焊接的 10 倍左右，印证了激光+GMAW 复合焊接相对 GMAW 的优越性.

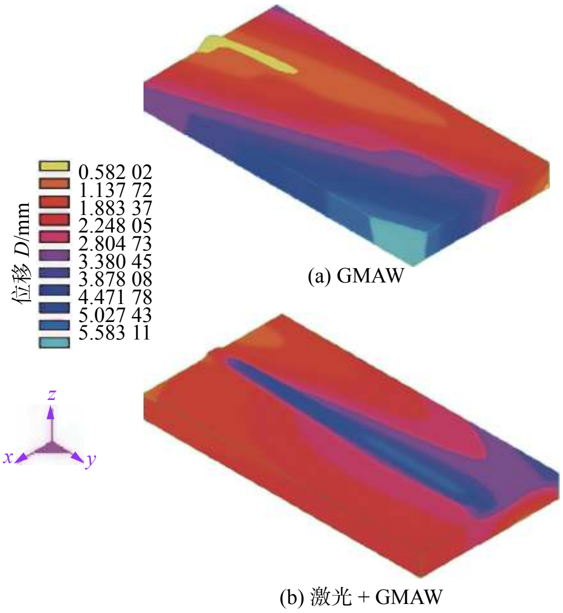

图 7 工件的整体变形

Fig. 7 Overall deformation of the workpiece. (a) GMAW; (b) laser+GMAW

2.3 残余应力

根据焊接应力的分布特点，分别对如图 8 所示的 3 条线上的残余应力结果进行提取分析. 其中，LINE 1 位于焊缝中心线上，LINE 2 位于焊趾处，LINE 3 位于焊板中心且垂直于焊缝. 图 9 ~ 图 11 分别为这 3 条线上的残余应力分布曲线. 从图 9 和图 10 可知，焊缝中心线 LINE 1 和焊趾处 LINE 2 在不同的焊接方法下所得到的残余应力分布规律大体相似. 对于纵向残余应力，由于焊缝两端为自由端，因此其值较小趋近于 0；而在焊缝中心位置有较大的纵向拉应力，且由于复合焊的热输入更为集

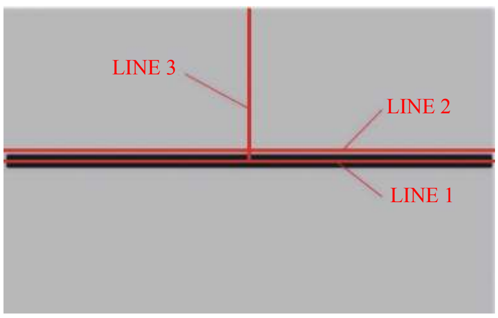

图 8 计算点的位置示意图

Fig. 8 Schematic diagram for calculated positions

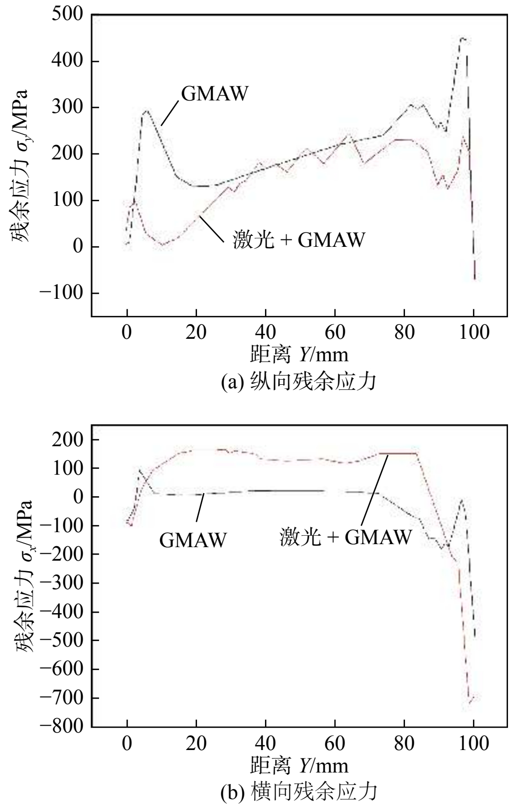

图 9　LINE 1 处的残余应力分布

Fig. 9　Residual stress distribution along LINE 1. (a) longitudinal direction ; (b) transverse direction

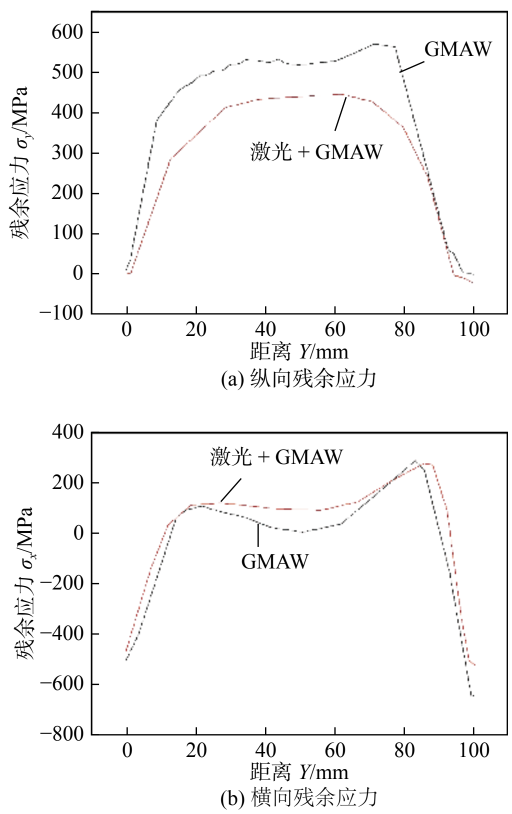

图 10　LINE 2 处的残余应力分布

Fig. 10　Residual stress distribution along LINE 2. (a) longitudinal direction; (b) transverse direction

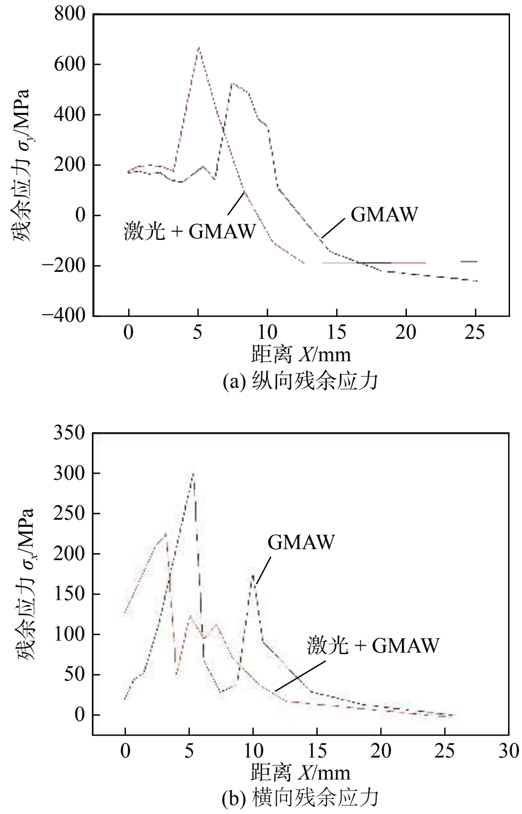

图 11　LINE 3 处的残余应力分布

Fig. 11　Residual stress distribution along LINE 3. (a) longitudinal direction; (b) transverse direction

中，在焊趾处 GMAW 比复合焊的纵向拉应力明显较大，但在焊缝处并不明显．而对于横向残余应力，在焊缝和焊趾的两端都表现出了较大的压应力．但由于复合热源焊接的焊缝熔宽较小，故焊缝中间位置所受横向残余应力相比于 GMAW 焊缝更为显著，而在焊趾处却相差不大．从图 11 中可以明显看出，LINE 3上复合焊和 GMAW 的应力都随着离焊缝的距离增大，应力先增大后减小．且复合焊比 GMAW 提前进入应力峰值，这是由于复合焊的焊缝熔宽较窄，焊趾尺寸较小，故复合焊高应力区范围相较于 GMAW 也较窄．焊缝及附近区域在高温时塑性变形，焊后受到拉应力的作用；而相对地，两侧远离焊缝的区域在整个热循环过程中未经历塑性变形，焊后受到压应力的作用．由此可见，对于复合焊与 GMAW 在相同的熔深条件下，复合焊的高应力区的范围明显的小于 GMAW．这是由于复合焊中，激光热输入较为集中且激光对电弧的收缩作用都更有利于获得较大的熔深．因此在获得相近熔深时，复合焊的送丝速度明显小于 GMAW，且复合焊的热输入仅为 GMAW的 0.29 倍，故产生的应力场也会相应的不同．

3 结 论

(1) 建立了适用于激光+GMAW 复合焊接工艺的“双椭球体热源+峰值递增圆柱体热源”的组合式体积热源, 数值计算的结果表明, 该热源模型能够准确预测工件的温度分布和焊缝横断面的形状尺寸.

(2) 利用焊接温度场的计算结果对 GMAW 和激光+GMAW 两种焊接工艺的焊接变形和焊后残余应力进行了计算. 结果表明, 复合热源焊接的焊接热输入、焊缝熔宽和工件的整体变形量等均比 GMAW 小. 此外, 复合热源焊接情况下的高应力区范围也有所降低.

参考文献

[1] Steen W M, Eboo M. Arc augmented laser welding[J]. Metal Construction, 1979, 11(7): 332 − 335.

[2] Steen W M. Arc augmented laser processing of materials[J]. Applied Physics, 1980, 51(11): 5636 − 5641.

[3] Dilthey U, Wieschemann A, Lueder F. Technical and economical advantages by synergies in laser arc hybrid welding[J]. Welding in the World, 1999, 43(4): 141 − 152.

[4] Shida T, Hirokawa M, Sato S. CO_2 laser welding of aluminum alloys-welding of aluminum alloys using CO_2 laser beam in combination with MIG arc[J]. Welding Research Abroad, 1997, 43(5): 36 − 41.

[5] Steen W M. Arc augmented laser welding-process variables, structure and properties[C]//The Joining of Metals, Spring Residential Conference, Coventry, 1981.

[6] Rejc J, Troyanova K, Iorio L, *et al*. Residual stresses prediction on clad pipeline girth welds through numerical simulation[J]. Procedia Manufacturing, 2019, 37: 605 − 612.

[7] Lu Y, Zhu S, Zhao Z, *et al*. Numerical simulation of residual stresses in aluminum alloy welded joints[J]. Journal of Manufacturing Processes, 2020, 50: 380 − 393.

[8] 逯世杰, 郑乔, 张超华, 等. 不同有限元软件对 Q390 钢厚板 T 型接头焊接残余应力和变形预测精度与计算效率的比较 [J]. 机械工程学报, 2019, 55(6): 11 − 12.

Lu Shijie, Zheng Qiao, Zhang Chaohua, *et al*. A comparative study on computational accuracy and efficiency of welding residual stresses and deformation in a Q390 steel thick plate T joint among three kinds of different FEM software[J]. Journal of Mechanical Engineering, 2019, 55(6): 11 − 12.

[9] Kong F, Ma J, Kovacevic R. Numerical and experimental study of thermally induced residual stress in the hybrid laser-GMA welding process[J]. Journal of Materials Processing Technology, 2011, 211(6): 1102 − 1111.

第一作者: 吴向阳，硕士；主要从事焊接工艺过程模拟仿真方面的研究和技术工作； Email：sfxiangyangw@163.com.
通信作者: 宿浩，博士； Email：suh@email.sdu.edu.cn.

（编辑： 胡广旭）

3. Chengdu AIGRE Technology Co., Ltd., Chengdu, 610097, China). pp 76-82

Abstract: For the shortcomings of the traditional power supply mode of the diesel generator set for the mobile flash welding machine, a new type of power supply system for the flash welding machine is presented. It is proposed to use a super capacitor to connect to a bidirectional DC/DC power converter in parallel with a battery pack through a switch to form a battery-supercapacitor hybrid energy storage system for driving mobile flash welding machines by analyzing the working characteristics of mobile rail flash welding machine. Established the model of hybrid energy storage system and conducted simulation tests, and test through product development of system prototypethe, the results show that the new hybrid energy storage system has fast dynamic response to load power ripple and stable output, which can not only meet the power supply requirements of rail flash welding machines, but also overcome the shortcomings of the three-phase load imbalance of the traditional diesel generator power supply mode and produce exhaust gas to pollute the environment. It has many advantages such as environmental protection. The independent research and development of the system has important reference significance for the technology upgrade and innovation of China seamless rail welding equipment.

Highlights: This system adopts the battery-supercapacitor hybrid energy storage power supply system to be successfully applied to the mobile flash rail welding machine for the first time, which replaces the existing power supply mode of diesel generator set, completely avoids the problems of unbalanced three-phase load and environmental pollution in the welding process, and has the advantages of energy saving, environmental protection and emission reduction.

Key words: mobile flash welding machines; battery; supercapacitor; hybrid energy storage system

Pressureless sintering behavior of nano-silver paste for large area chip interconnection WU Weizhen, YANG Fan, HU Bo, LI Mingyu (Sauvage Laboratory for Smart Materials, Harbin Institute of Technology (Shenzhen), Shenzhen, 518055, China). pp 83-90

Abstract: A nano-silver paste which can be used in low temperature sintering was prepared by chemical reduction method. By analyzing the microstructure, mechanical properties and failure modes of pressureless low temperature sintered nano-silver joints, the gradual microstructure evolution of the pressureless sintered silver joints was systematically discussed, and the influence of joint size on the connection performance and reliability of sintered silver was obtained. By heating the joint to 250 ℃ with the sintering time of 1 hour, the shear strength of pressureless sintered joint reached 70 MPa or more when the joint area was less than or equal to 3 mm × 3 mm. As the joint area increased, the shear strength of the solder joint gradually decreased. However, when the solder joint size was 10 mm × 10 mm, the shear strength remained above 20 MPa. The fracture interface morphology showed that the larger the joint area, the lower the plastic deformation of the sintered silver. It was interesting that there was a gradual microstructure evolution from the center to the edge of the joints of all sizes, and violent plastic deformation occurred at the edges.

Highlights: (1) The nano-silver paste with the optimized organic coating was used to realize the pressureless low temperature sintering connection of a large area chip (10 mm × 10 mm).
(2) The influence of the size of interconnect joints on the microstructure and echanical properties of the sintered silver was illustrated. The gradual microstructure evolution of sintered silver microstructure in pressureless joints was obtained.

Key words: nano-silver paste; pressureless sintering; large area; mechanical properties; microstructure evolution

Thermal-mechanical coupled numerical analysis of laser + GMAW hybrid heat source welding process WU Xiangyang[1], SU Hao[2], SUN Yan[2], CHEN Ji[2], WU Chuanong[2] (1. CRRC Qingdao Sifang Co., LTD., Qingdao, 266111, China; 2. MOE Key Lab for Liquid-Solid Structure Evolution and Materials Processing, Institute of Materials Joining, Shandong University, Jinan, 250061, China). pp 91-96

Abstract: From the viewpoint of macroscopic phenomena in heat transfer, a combined "double-ellipsoid + linearly-increased peak value cylinder" volumetric heat source distribution mode was proposed according to the characteristics of laser + GMAW hybrid heat source welding process. A finite element model of laser + GMAW hybrid heat source welding process was established. The temperature distribution, and the size of the weld cross-section were numerically calculated. It can be observed that the calculated results were in good agreement with the experimental results, which proves the rationality and applicability of the combined volumetric heat source model. And then, the calculated temperature field was utilized for the numerical modeling and comparison of the welding deformation and residual stress between GMAW and laser + GMAW hybrid welding process. The results shown that the heat input, weld width, welding deformation and high residual stress region of laser + GMAW hybrid welding were all much smaller than that of GMAW with the identical weld pool depth. The research confirmed the advantages of laser + GMAW hybrid welding, and provided basic theoretical data for the optimization of process parameters.

Highlights: (1) A combined heat source model for laser + GMAW hybrid welding was established, and the distributions of temperature and residual stress on the workpiece were numerically calculated.

(2) It was shown that heat input, weld width and range of high stress zone for laser + GMAW were all smaller compared with that for GMAW under the same weld penetration, which confirmed the superiority of the hybrid heat source welding process.

Key words: hybrid welding; combined volumetric heat source; thermal-mechanical coupling; numerical analysis